Hypometabolism to survive the long polar night and subsequent successful return to light in the diatom Fragilariopsis cylindrus

Nathalie Joli, Lorenzo Concia, Karel Mocaer, Julie Guterman, Juliette Laude, Sebastien Guerin, Theo Sciandra, Flavienne Bruyant, Ouardia Ait-mohamed, Marine Beguin, et al.

New Phytologist

Research

Hypometabolism to survive the long polar night and subsequent successful return to light in the diatom *Fragilariopsis cylindrus*

Nathalie Joli[1], Lorenzo Concia[1]*, Karel Mocaer[2]*, Julie Guterman[1†], Juliette Laude[1†], Sebastien Guerin[3], Theo Sciandra[1,3], Flavienne Bruyant[3], Ouardia Ait-Mohamed[1], Marine Beguin[3], Marie-Helene Forget[3], Clara Bourbousse[1], Thomas Lacour[4], Benjamin Bailleul[5], Charlotte Nef[1], Mireille Savoie[6], Jean-Eric Tremblay[7], Douglas A. Campbell[6], Johann Lavaud[3,8], Yannick Schwab[9], Marcel Babin[3] and Chris Bowler[1]

[1]Institut de Biologie de l'École Normale Supérieure (IBENS), École Normale Supérieure, CNRS, INSERM, PSL Université Paris, 75005, Paris, France; [2]Cell Biology and Biophysics Unit, European Molecular Biology Laboratory (EMBL) & Collaboration for Joint PhD Degree between the European Molecular Biology Laboratory and the Heidelberg University, Faculty of Biosciences, 69117, Heidelberg, Germany; [3]Takuvik International Research Laboratory, Université Laval (Canada) & CNRS (France), Département de Biologie and Québec-Océan, Université Laval, Québec, QC, G1V 0A6, Canada; [4]Laboratoire PHYSiologie des micro ALGues (PDG-ODE-PHYTOX-PHYSALG), Centre Atlantique, 44 311, Nantes, France; [5]Laboratory of Chloroplast Biology and Light Sensing in Microalgae, Institut de Biologie Physico Chimique, CNRS, Sorbonne Université, Paris, 75005, France; [6]Département de Biologie, Université Laval, Québec, QC, G1V 0A6, Canada; [7]Mount Allison University, Sackville, NB, E4L 1H3, Canada; [8]UMR 6539 LEMAR-Laboratory of Environmental Marine Sciences, CNRS/Univ Brest/Ifremer/IRD, IUEM-Institut Européen de la Mer, Technopôle Brest-Iroise, rue Dumont d'Urville, 29280, Plouzané, France; [9]Cell Biology and Biophysics Unit and Electron Microscopy Core Facility, European Molecular Biology Laboratory (EMBL), 69117, Heidelberg, Germany

Authors for correspondence:
Nathalie Joli
Email: joli@biologie.ens.fr

Marcel Babin
Email: marcel.babin@takuvik.ulaval.ca

Chris Bowler
Email: cbowler@biologie.ens.fr

Received: *20 June 2023*
Accepted: *17 October 2023*

New Phytologist (2023)
doi: 10.1111/nph.19387

Key words: autophagy, diatom, energy homeostasis, *Fragilariopsis cylindrus*, polar night, quiescence.

Summary

- Diatoms, the main eukaryotic phytoplankton of the polar marine regions, are essential for the maintenance of food chains specific to Arctic and Antarctic ecosystems, and are experiencing major disturbances under current climate change. As such, it is fundamental to understand the physiological mechanisms and associated molecular basis of their endurance during the long polar night.
- Here, using the polar diatom *Fragilariopsis cylindrus*, we report an integrative analysis combining transcriptomic, microscopic and biochemical approaches to shed light on the strategies used to survive the polar night.
- We reveal that in prolonged darkness, diatom cells enter a state of quiescence with reduced metabolic and transcriptional activity, during which no cell division occurs. We propose that minimal energy is provided by respiration and degradation of protein, carbohydrate and lipid stores and that homeostasis is maintained by autophagy in prolonged darkness. We also report internal structural changes that manifest the morphological acclimation of cells to darkness, including the appearance of a large vacuole.
- Our results further show that immediately following a return to light, diatom cells are able to use photoprotective mechanisms and rapidly resume photosynthesis, demonstrating the remarkable robustness of polar diatoms to prolonged darkness at low temperature.

Introduction

In polar regions, resident species must cope with difficulties such as year-round cold, continuous light around summer solstice and continuous darkness around winter solstice, but those species that can cope are present in large numbers of individuals (Blix, 2016; Ibarbalz *et al.*, 2019). Hypometabolism is a frequent strategy to survive in the face of various environmental stresses with one of the most extreme examples being mammalian hibernation (Storey & Storey, 2007), consisting of a general reduction in metabolism that allows a conservation of energy during the winter months. The ability of phytoplankton, which are the basis of the marine food chain, to survive during the polar night, despite the prolonged near-absence of light, has been known for over 30 yr (Dehning & Tilzer, 1989; Reeves *et al.*, 2011). The size of the surviving population of over-wintering phytoplankton is thought to impact the level of primary production once light is again available in spring, after annual sea ice break-up (Palmisano & Sullivan, 1983).

Survival in prolonged darkness by microalgae most commonly involves a physiological resting state, as opposed to spore

*These authors contributed equally to this work.
†These authors contributed equally to this work.

production, which appears to be uncommon, and to mixotrophy, for which long-term survival is uncertain (Hoban *et al.*, 1980; McMinn & Martin, 2013). As a function of responses to shorter or longer periods of darkness, a resting physiological state has been described in chlorophytes (Hellebust & Terborgh, 1967; Dehning & Tilzer, 1989; Baldisserotto *et al.*, 2005a; Ferroni *et al.*, 2007), pelagophytes (Popels *et al.*, 2007), temperate (Handa, 1969; Griffiths, 1973) and polar diatoms (Palmisano & Sullivan, 1982; Peters & Thomas, 1996; Reeves *et al.*, 2011; Mock *et al.*, 2017; Schaub *et al.*, 2017; Lacour *et al.*, 2019; Morin *et al.*, 2020), as well as in xanthophytes (Baldisserotto *et al.*, 2005b) and rhodophytes (Lüder *et al.*, 2002). Overall, the observations suggest a low rate of metabolic activity with limited consumption of reserves, partial dismantling of the photosynthetic apparatus and reduction in the photosynthetic performance during darkness.

High-latitude phytoplankton biomass is dominated by unicellular diatoms (Pierella Karlusich *et al.*, 2020). These photosynthetic Stramenopiles have chloroplasts derived from secondary endosymbiosis as well as a combination of host- and endosymbiont-derived genes in their nuclear genome (Bowler *et al.*, 2010), and an external cell wall, or frustule, made of silica. Diatoms play key roles in the global carbon and silica cycles in the ocean (Tréguer *et al.*, 2021), accounting for about half of marine primary production (Field *et al.*, 1998). The capacity of diatoms to withstand fluctuating environments, including the highly variable light conditions in polar oceans, may be key to their ecological success (Lacour *et al.*, 2018; Croteau *et al.*, 2021, 2022).

Diatom light-harvesting pigments differ significantly from those of green algae and plants, and include chlorophyll *c*, fucoxanthin and the photoprotective pigments diadinoxanthin and diatoxanthin (Olaizola *et al.*, 1994) and also possess gene subfamilies encoding light-harvesting complex proteins, LHCx and LHCz, believed to enhance photosynthetic light capture under variable environmental conditions (Goss & Lepetit, 2015). Furthermore, they are equipped with a suite of, sometimes unique, photoreceptors that finally regulate the sensing of the complex marine light climate to improve the global light acclimation (Falciatore *et al.*, 2022), including the cryptochrome photolyase family, which has both DNA repair and photoreceptor activities (Coesel *et al.*, 2009).

Fragilariopsis cylindrus is among the most successful taxa in the Southern Ocean (Malviya *et al.*, 2016) and a reference genome is available for it (Mock *et al.*, 2017). Having adapted to low light conditions as found under sea ice, *F. cylindrus* is thus a valuable model organism to explore life in the polar environment. Dark survival of *F. cylindrus* has received attention, and some authors (Morin *et al.*, 2020) have monitored multiple physiological and metabolic traits in the dark and light return while others have characterized gene expression without physiological analyses, and without monitoring of postdarkness recovery in the light (Mock *et al.*, 2017). Recently, a respiratory metabolism of dark-acclimated cells based mostly on proteomic profiling has been proposed (Kennedy *et al.*, 2019). We nonetheless lack an integrated understanding of how this diatom survives the long polar night.

Here, we describe experimental set-ups that combine microscopic, transcriptomic and biochemical approaches to assess the survival strategies of polar diatoms during a prolonged period of darkness and subsequent re-exposure to light. Our results support suggestions of entry into a resting physiological state during prolonged darkness made in previous studies. We also propose strategies involving specific genes and metabolic pathways involved in the ability of *F. cylindrus* to survive the long polar night.

Materials and Methods

Experimental design

Triplicate cultures of *Fragilariopsis cylindrus* CCMP 3323 were kept homogeneous through agitation with a magnetic stirrer in Aquil media (Morel *et al.*, 1979) in a cold room at 0 ± 1°C in 80 l glass cylinders (diameter: 30 cm, height: 140 cm; Sciandra *et al.*, 2022). After a period of acclimation at 30 µmol photon $m^{-2}\,s^{-1}$ (DURIS® E3 LED bands GW JCLMS1.EC, 4000 K) in semi-continuous cultivation, cultures reached a cell concentration close to 10^6 cells ml^{-1} in a final volume of 80 l and were transferred to total darkness in a closed system. Growth of bacteria was minimized by adding streptomycin (100 mg l^{-1}), kanamycin (100 mg l^{-1}), antimycin (100 mg l^{-1}) and gentamycin (50 mg l^{-1}) to the medium before the final volume increase. During the darkness period, samplings were performed under green room lighting (LEE filter #740; 0.1 µmol photon $m^{-2}\,s^{-1}$).

Most of the parameters were measured on the cylinders described above, with the exception of the quantification of photosynthetic proteins, performed on another set of cylinders that were kept in the dark for 1 month under identical conditions. The cells used for RNA polymerase immunoblots, and electron and confocal microscopy were from independent cultures in 300 ml flasks that spent 1–2 months in the dark at 4°C (Supporting Information Table S1).

Sample preparation and microscopy acquisition

For scanning electron microscopy (SEM) and focused ion beam-scanning electron microscopy (FIB-SEM), cells were fixed in 2.5% glutaraldehyde and 4% paraformaldehyde in 0.15 M marPHEM buffer (Montanaro *et al.*, 2016) for 72 h then transferred to 0.15 M PHEM containing 4% paraformaldehyde. For SEM, cells were washed and pipetted onto a 0.65 µm mesh filter (MF-Millipore, DAWP02500) before air drying and imaged with a Zeiss CrossBeam 540. For FIB-SEM, cells were washed before being aspirated into cellulose capillaries (Wohlwend GmbH, Sennwald, Switzerland). Samples were cryofixed using an HPM010 (AbraFluid, Widnau, Switzerland). Freeze-substitution and resin embedding were performed (Ronchi *et al.*, 2021) in an AFS2 machine (Leica Microsystems, Vienna, Austria) and image acquisition with a Zeiss CrossBeam 550. Image stacks were aligned using an AMST workflow (Hennies *et al.*, 2020). Segmentation was done using Microscopy Image Browser and morphometric analysis and visualization using Amira (Thermo Fisher Scientific, Waltham, MA, USA; Videos S1–S6).

For transmission electron microscopy (TEM), cells were cryo-fixed (HPM100; Leica Microsystems) and freeze substituted (EM-AFS2; Leica microsystems) using the following steps: 98 h at −90°C in 0.1% tannic acid and 0.5% glutaraldehyde in acetone and washed with acetone at −90°C, 32 h at −90°C in 2% osmium tetroxide in acetone; temperature was −20°C over 14 h (5°C h^{-1}), −20°C over 16 h and then raised to 4°C over 4 h (6°C h^{-1} HR) and washed with acetone at 4°C. The cells were then infiltrated with EPON hard resin. The resin (without accelerator)/acetone (v/v) series used were 25% for 2 h starting at 4°C and reaching 20°C (8°C every hour), 50% and 70% each for 2 h at 20°C. Infiltration with 100% resin (with accelerator) was then performed three times for 3 h and once O/N before polymerization at 60°C for 48 h. Seventy-nanometre thin sections were obtained using an ultramicrotome (Leica EM) with an ultra-diamond knife (Diatome, Nidau, Switzerland). Two by two tiles were acquired semi-automatically on the JEOL JEM 2100plus using 120 kV and ×8000 magnification. Micrographs were processed using FIJI, and tiles were stitched using PHOTOSHOP.

Confocal microscopy was performed using a Leica TCS SP8. Cells were stained with NileRed in their culture medium (Merck – Sigma-Aldrich #72485-100MG) at a final concentration of 2.5 ng ml^{-1} for 20 min in the dark, and then pelleted and resuspended in DAPI (4′,6-Diamidino-2-Phenylindole, Dihydrochloride; Thermo Fisher #D1306), at a final concentration of 0.1 mg ml^{-1}.

TEM analysis and statistical analyses

A total of 86 Light and 99 Dark images were randomly picked and analysed. All quantitative measurements were performed using FIJI v.2.3.0/1.53f, with either the free-hand tool or the line tool. Heterochromatin vs euchromatin ratio was measured by binarizing the nucleus and counting the number of dark over white pixels (Cherkezyan *et al.*, 2014). The nucleolus has been considered independently. If the repartition of a given feature of interest followed a normal distribution (Shapiro test), means were compared with a two-sided Student *t*-test considering whether the two populations' variances were equal or not upon the result of a Fisher exact test. Otherwise, if the populations compared were large enough ($n_i > 30$), means were compared with a two-sided Student *t*-test with populations' variances considered unequal. Otherwise, a nonparametric two-sided Wilcoxon test was performed. All tests' results are given with a 5% confidence level. ns stands for not significant; *, $0.01 \leq P < 0.05$; **, $0.001 \leq P < 0.01$; ***, $P < 0.001$.

Biochemistry and cytometry measurements

Number and size distribution of phytoplankton cells were determined, along with the estimation of bacterial contamination (SYBR Green), cell viability (SYTOX Green) and neutral lipids (BODIPY) content assessed by flow cytometry (Sciandra *et al.*, 2022). Macronutrient concentrations were determined (Sciandra *et al.*, 2022).

Respiration rates of the cultures were assessed by measuring the change in dissolved oxygen concentration in the dark for 1 h, using optical sensors (FireSting®-O_2; Pyro Science GmbH, Aachen, Germany). The sample was gently stirred to avoid cell sinking during the measurement. Sampling bottles were airtight with the measuring probe applied through the stopper. Data were fitted with respiration (in µmol O_2 l^{-1} h^{-1}) being the slope of a linear model.

Concentrations of photosynthetic and nonphotosynthetic pigments were determined by HPLC (Ras *et al.*, 2008). The de-epoxidation state (DES, in %) was calculated as:

$$\mathrm{DES} = \frac{\mathrm{DT}}{\mathrm{DD} + \mathrm{DT}} \times 100$$

where DT is diatoxanthin and DD is diadinoxanthin (in mol per 100 mol chlorophyll *a*).

Photosynthetic performance

All the photosynthetic measurements were made at 0 ± 1°C under green room lighting. A triplicate of dark-acclimated (30 min) sample was submitted to a blue light saturating flash (100 µs, 455 nm) in a fluorescence induction and relaxation (FIRe) fluorometer (Satlantic, Halifax, NS, Canada). The photosystem II (PSII) absorption cross-section (σ_{PSII}) was calculated following Kolber *et al.* (1998).

A red light source ($\lambda = 655$ nm) pulse amplitude modulated fluorometer (PHYTO-PAM with PHYTO-ED unit, Walz, Germany) was used to measure the photosynthetic performance of cells on dark-acclimated samples. Rapid light curves (RLCs) were performed with 13 steps of 30 s (from 0 to 490 µmol photons m^{-2} s^{-1}). The photochemical efficiency of PSII, F_V/F_M was calculated as:

$$F_V/F_M = \frac{F_M - F_0}{F_M}$$

where F_0 and F_M are, respectively, the minimum and maximum levels of dark-acclimated chlorophyll fluorescence. The relative electron transport rate (rETR) was calculated as:

$$\mathrm{rETR} = E \times \frac{F'_M - F'}{F'_M}$$

where E is the light intensity, and F' and F'_M are, respectively, the minimum and maximum levels of light-acclimated chlorophyll fluorescence. rETR vs E curves were fitted according to Eilers & Peeters (1988) in order to extract rETR_{max}, the maximum relative electron transport rate (Barnett *et al.*, 2015). The output of the RLCs also allowed to calculate the nonphotochemical quenching (NPQ) as:

$$\mathrm{NPQ} = \frac{(F_M - F'_M)}{F'_M}$$

The maximal NPQ (NPQ_{max}) was the maximal value obtained for the highest RLC step (Serôdio & Lavaud, 2011).

Photosynthetic parameters were further determined by measuring the ^{14}C-uptake of phytoplankton samples exposed at 24 light levels (from 0 to 800 µmol photon $m^{-2}\,s^{-1}$; Morin *et al.*, 2020; Croteau *et al.*, 2021). Raw data were fitted to the model of Platt *et al.* (1981) and allowed to determine the light saturation coefficient in µmol photons $m^{-2}\,s^{-1}$ ($P-E_K$), the chlorophyll-specific photosynthetic efficiency coefficient in mgC mg Chl$a^{-1}\,h^{-1}$ per µmol photon $m^{-2}\,s^{-1}$ ($P-\alpha$), and the maximum specific carbon fixation rate in mgC mg Chl$a^{-1}\,h^{-1}$ ($P^B{}_{max}$).

Molecular biology procedures

Photosynthetic protein quantification (RuBisCo (RbcL) and protein D1 (PsbA)) was done by immunoquantitation as described previously (Morin *et al.*, 2020), with total protein quantitation done using a Bicinchoninic Acid (BCA™) protein assay with bovine gamma globulin protein standard.

Chromatin was extracted (Lin *et al.*, 2012), and we used the RNA pol II CTD phospho Ser2 antibody (AbFlex 91115) that binds to the active form of RNA Polymerase II to do immunoblot (6% acrylamide, transfer at 30 V overnight). Histone H4 was used as a loading control. Quantification of the blot was performed using the mean grey value on FIJI, using amount as a ratio of each protein band relative to the lane's loading control.

RNA was isolated following the protocol of the manufacturer using the RNeasy Mini Kit (Qiagen). A second DNase step was added after elution (DNase Invitrogen™ Kit TURBO DNA-free). Library preparation was made using Illumina TruSeq Stranded mRNA Library Prep including poly-A selection and performed at the biotechnology company Fasteris along with sequencing that yields > 30 million reads per sample (Illumina Sequencing HiSeq 4000, 2× 150 bp).

Reference genome and bioinformatics

From the reference genome (Mock *et al.*, 2017), we removed genes that overlap with transposable elements and worked with a final set of 23 902 genes (Dataset S1). We ran a *de novo* repeat detection using the TEdenovo pipeline from the REPET package v.2.4 (Flutre *et al.*, 2011). This library of consensus sequences was then used as a digital probe for whole-genome annotation by the TEannot (Quesneville *et al.*, 2005; Dataset S2).

Raw data were deposited at https://www.ncbi.nlm.nih.gov/geo/ under the GEO accession no. GSE218215. The quality was verified with FASTQC v.0.11.9 and aligned to the reference genome using STAR v.2.7.9a. Raw read counts over exons were obtained with htseq-counts v.0.13.5 and used for differential expression analysis and principal component analysis with DESEQ2 v.1.26.0 against T0LIGHT. Macrotrends of gene expression were defined with the Dynamic Regulatory Events Miner, DREM v.2.0 (Schulz *et al.*, 2012) taking in account genes differentially expressed compared with T0LIGHT ($|\log_2 FC| > 2$, $P < 0.01$) in at least two consecutive time points. Subclusters of genes within each macrotrend were identified with the function kmeanspp of the package LICORS v.0.2.0.

The R package TOPGO was used to determine the gene ontology terms enrichment (Fisher's exact test, $P < 0.05$) and used CIRGO to visualize them. The KAAS –KEGG Automatic Annotation Server (Moriya *et al.*, 2007) was used for ortholog assignment. *In silico* targeting predictions were performed using HECTAR and ASAFIND v.2.0.

Tara Oceans is a planetary-scale project in which the taxonomic composition of protist communities was characterized through DNA metabarcoding using the V9 region of the 18S rRNA gene (Ibarbalz *et al.*, 2019) (https://zenodo.org/record/3768510#.Ye-xqpHMJzp). To explore the distribution and contribution to local diatom communities of the diatom genus *Fragilariopsis*, we pooled together *Fragilariopsis*-specific sequences from all the eukaryote-enriched size fractions (Pierella Karlusich *et al.*, 2020; 0.8–5; 5–20; 20–180 and 180–2000 µm) and from two epipelagic layers (surface and deep-chlorophyll maximum). The data were normalized against the total reads assigned to diatoms within each sample, which corresponds to the proportion of *Fragilariopsis* reads to diatom communities. Results were plotted using the R package MAPDATA v.2.3.0.

Results

Fragilariopsis distribution in *Tara* Oceans using metabarcoding data

To investigate whether the diatom genus *Fragilariopsis* could be identified within natural communities experiencing prolonged darkness and to better explore its importance within diatom communities, metabarcoding data corresponding to the *Fragilariopsis* genus from 141 distinct *Tara* Oceans stations were retrieved, including 20 stations from the Arctic Ocean. Compared with a previous study (Malviya *et al.*, 2016) describing the cosmopolitan genus *Fragilariopsis*, our analysis here includes new sampling stations from the Arctic Ocean and shows that *Fragilariopsis* indeed occurs at high latitudes (> 72°N) that experience prolonged darkness, where it can significantly contribute up to 30% to diatom populations (Fig. S1; Table S2).

Cellular bioenergetics during initial full light, prolonged darkness and subsequent return to light

Fragilariopsis cylindrus cultures acclimated to continuous light were subjected to darkness for a period of 86 d, followed by re-exposure to continuous light for 7 d. Parameters measured are summarized in Table S1. We first explored bulk and within-cell biochemical and photophysiological changes. During the first 3 d of darkness, cell abundance increased up to 30%, likely from the completion of a last division. *F. cylindrus* then stopped cell division in the dark (Figs 1a, S2a). Viability as determined by cytometry remained high (99%) during the dark period. Upon light return, cell mortality of 30% occurred during the first 3 d (Fig. S2b). Subsequently, an increase in cell number was consistent with cell division exceeding the initial mortality losses.

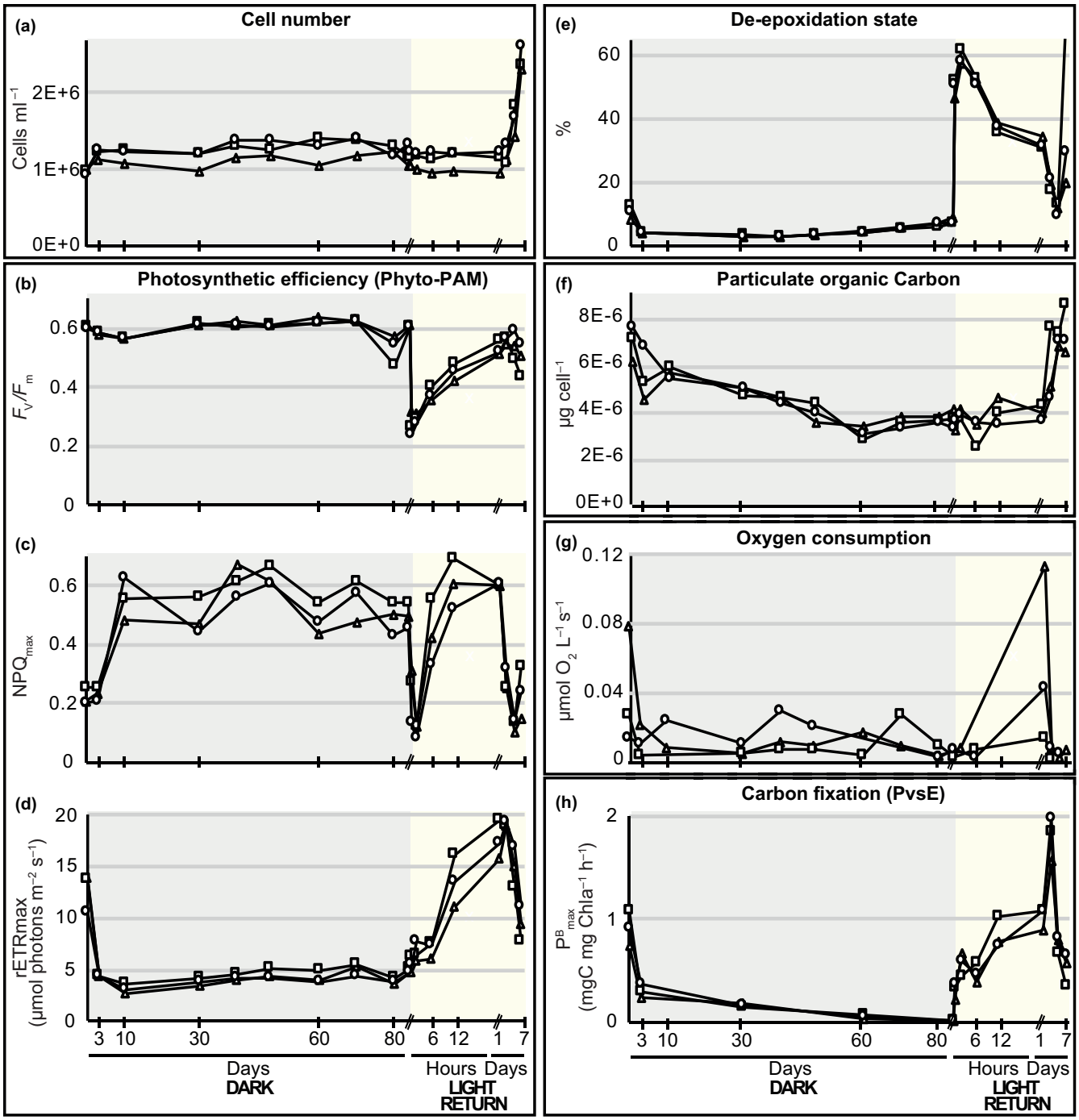

Fig. 1 Tracking physiological changes in *Fragilariopsis cylindrus* from the acclimation phase in full light, to prolonged darkness (grey area of the graphs), and upon return to light (yellow area of the graphs). (a) Number of cells ml^{-1}. (b) Maximum quantum yield of photosystem II (F_V/F_M). (c) Nonphotochemical quenching (NPQ_{max}). (d) Maximum relative photosynthetic electron transport rate ($rETR_{max}$, µmol photons m^{-2} s^{-1}). (e) De-epoxidation state (DES, %). (f) Carbon content (µg $cell^{-1}$). (g) Oxygen consumption (µmol O_2 l^{-1} s^{-1}). (h) Maximum chlorophyll-specific carbon fixation rate in mgC mg $Chla^{-1}$ h^{-1} (P^B_{max}). The three biological replicates are represented with triangles (Cylinder 1), squares (Cylinder 2) and circles (Cylinder 3). *X*-axis shows the time points sampled with a broken scale in hours or days. See Supporting Information Table S1 and Fig. S2 for all the time points sampled per parameter.

Bulk particulate carbon and nitrogen concentrations, together with photosynthetic pigments per cell (Chl*a*, Chl c2 and Fx), decreased by half during the dark period (Figs 1f, S2d, S2f). Lipid content as estimated by cytometry also gradually decreased during prolonged darkness (Fig. S2b). We observed a general decrease in oxygen consumption after 3 months of darkness, at 2 to 13 times lower than the rates measured from light-acclimated cells before the dark period (Figs 1g, S2e). Within 2 h of the return to light, the de-epoxidation state of xanthophyll cycle pigments (DES = DT/(DD + DT) × 100) reached a maximum of 60%, illustrating the induction of photoprotection (Figs 1c,e, S2g). While lipid stocks replenished within the first 2 d of light return,

particulate carbon and nitrogen, as well as photosynthetic pigment stocks, only returned to baseline after 5 d light return.

The maintenance of a high F_V/F_M aligned with a slight decrease in σPSII in prolonged darkness (Figs 1b, S2h, S2i). As the cylinders were maintained in a closed system throughout the experiment, cultures grew exponentially when light returned until they were limited by nutrient availability. This had an impact on the 'light-adapted' parameters that became apparent between Days 5 and 7 following the return to light, such as DES and F_V/F_M values (Fig. S2c).

Morphological changes in *F. cylindrus* in continuous light and after prolonged darkness

We then assessed the morphological responses of *F. cylindrus* to prolonged darkness using SEM, TEM and FIB-SEM and confocal microscopy, performed on light- and dark-acclimated cells (Table S1). Scanning electron microscopy did not reveal major external differences between light- and dark-acclimated cells, indicating that *F. cylindrus* does not form spores in the dark (Kuwata *et al.*, 1993; McQuoid & Hobson, 1996; Figs 2a,b, S3a, b). The FIB-SEM and TEM revealed, however, significant changes in cell constitution, including the *de novo* formation of a large vacuole in prolonged darkness (Figs 2d,f, 3a).

Focused ion beam-scanning electron microscopy results take into account the total volume of each cell (measured for up to five cells). Transmission electron microscopy images, on the contrary, reflect the proportions of a given organelle or feature visible from a cell thin section, and measurements from these images must therefore be taken with caution (up to 99 cells). The large vacuole occupied 25% of the cell volume as estimated by FIB-SEM, or 40% of the projected area as estimated by TEM (Figs 3b, S4). In agreement with cell counts, TEM analysis showed significantly fewer dividing cells from dark-acclimated populations ($P < 0.001$; Fig. S3e). In line with the cytometry results (BODIPY), TEM image analysis also showed a decrease in the number and size of dense-core organelles ($0.001 \leq P < 0.01$) that we consider to be storage lipid droplets. By NileRed staining with confocal microscopy, we also observed fewer lipid droplets in the dark than in the light (Figs 3c,d, S5). Furthermore, we observed electron lucent spherical organelles that could potentially be chrysolaminarin stock, the major carbohydrate food reserve of diatoms (Chiovitti *et al.*, 2004; or could be empty lipid droplets; Fig. S3c). In addition, a higher ratio of heterochromatin to euchromatin was found in the dark which, in conjunction with the smaller size of the nucleus ($0.001 \leq P < 0.01$), suggests that the DNA is more condensed and less accessible for gene transcription (Fig. 3f,g). Of the explored nuclei, we found fewer and smaller nucleoli (ribosome factories) in the dark ($0.001 \leq P < 0.01$; (Fig. S3h), which may underlie the decreased metabolic activity.

Gene expression clustering and enriched functions

To explore temporal changes in gene expression, we sequenced a total of 48 transcriptomes from cultures that span the time series from the full-light acclimation phase (T0LIGHT), through darkness to the light return phase (Table S1). Principal component analysis revealed a gradual transition in gene expression, first from 6 h to 6 d of darkness (short-term darkness), and then from 6 d to 1 and 2 months of darkness (long-term darkness). We noted a continuous change in gene expression from 30 min to 2 h of return to light (short-term response to light) to 6 h to 1 d of return to light (longer-term response). The return to the initial state of gene expression consistent with T0LIGHT was again observed after 2 d of light return (Fig. 4a). A maximum of 35% of the total number of genes were downregulated in the dark whereas *c.* 7% were upregulated ($|\log_2 FC| > 2$, $P < 0.01$), relative to T0LIGHT. Following return to light, expression of *c.* 32% of genes were affected during the first day (12% up and 20% down). In comparison, *c.* one-third of the genome of Arabidopsis is regulated during de-etiolation, with three-fifths upregulated and two-fifths downregulated by light (Ma *et al.*, 2001). Using the Dynamic Regulatory Events Miner approach, we could identify five temporal macro trends (clusters) in gene expression over 14 853 genes (62% of the total number of genes) as compared to T0LIGHT. Clusters were then subdivided into subclusters (Fig. 4b,c; Table S3).

The enriched functions within subclusters 1A to 1C suggest that the cell repairs DNA after 30 min of light return, and that genes involved in gene expression and ribosome biogenesis remain active up to 3 d of darkness, switch off in prolonged darkness, and turned on again after 6 h of light return. Subcluster 1D, upregulated throughout the dark period and losing expression to return to baseline 3 d after light return, is enriched in genes involved in apoptotic processes. Subclusters 2A and 2C have similar temporal trends, with downregulation in the dark and increased expression from 12 h after light return, and are enriched in functions such as gene expression, translation and fatty acid synthesis. The enriched functions within subcluster 2B suggest that DNA replication restarts from 30 min after light return. The subclusters 3A to 3C are genes that recover the same expression level as T0LIGHT starting from 1 to 2 d after light return. They are enriched in genes involved in photosynthesis, chlorophyll synthesis and cell division. Subclusters 4A and 4B comprise genes that were overexpressed during the early darkness and are enriched in genes involved in chromatin organization, lipid and carbohydrate catabolism. Subcluster 4C contains genes that are induced throughout the dark period as compared to T0LIGHT and is enriched in functions such as respiration (including the alternative oxidase (AOX)-dependent respiration pathway genes; Fig. 4c). The smallest Cluster 5 is made up of genes downregulated throughout the experiment compared with T0LIGHT and, unlike all other clusters, these genes do not return to the initial state after 7 d of light return. The gene ontologies detected in this cluster include signal transduction, transcription and response to wounding (not illustrated here; Table S3).

To detect fast variations in expression that could have been missed in the macrotrends analysis, we examined genes that were differentially expressed at single time points as compared to T0LIGHT. The list includes 3619 genes (15% of total number of genes) among which one-third are specific to 30 min light return. Among the enriched Gene Ontology categories, we found cell communication, mRNA and protein metabolism, and cytochrome

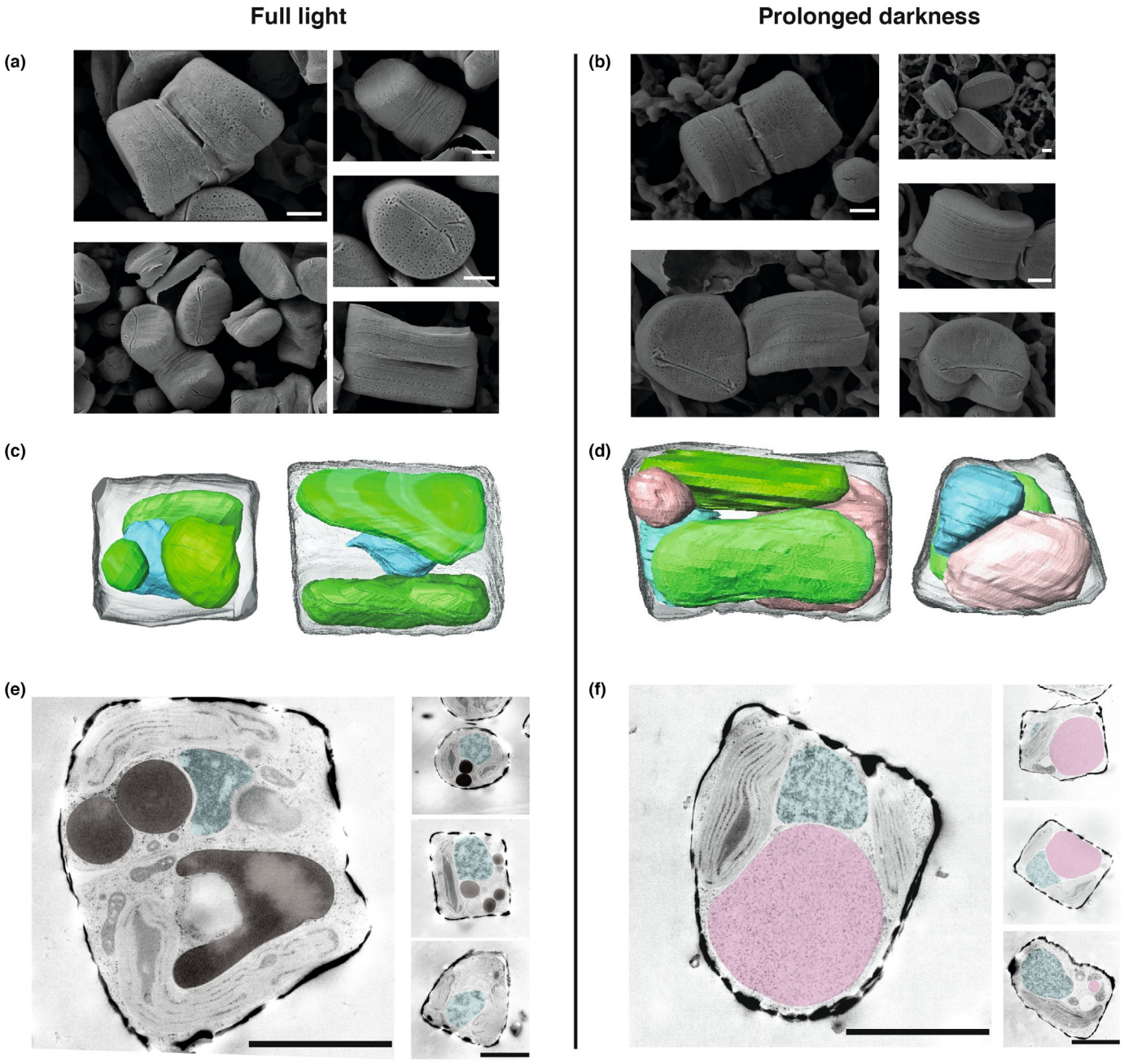

Fig. 2 Morphological differences between *Fragilariopsis cylindrus* from continuous light and after prolonged darkness. (a) Outer cell morphology observed by scanning electron microscopy (SEM) from continuous light and (b) after prolonged darkness. (c) 3D cell reconstruction with false colour from focused ion beam-scanning electron microscopy (FIB-SEM) from continuous light and (d) after prolonged darkness. Chloroplasts are in green, the nucleus in light blue and the vacuole in pink (see Supporting Information Videos S1–S6). (e) Inner cell morphology observed by transmission electron microscopy (TEM) from continuous light and (f) after prolonged darkness, with false colour. Putative lipids are in brown, the nucleus in light blue and the vacuole in pink. Bars, 1 µm.

complex assembly. A total of 194 genes were specifically differentially expressed after 3 d of darkness; the enriched gene ontology functions include apoptosis (Fig. S6; Table S4).

Integrative view of cell metabolism in the dark and following light return

We explored metabolic pathways by relating patterns of gene expression (samples merged according to Fig. 4a) with the corresponding biochemical results when available. The results are summarized in Fig. 5. The timing of the transition from short-term to long-term dark response at the transcriptomic level is consistent with the stabilization of cell counts in the culture, along with the decrease in $rETR_{max}$, P^{B}_{max} and in the contents of the photosynthetic proteins RbcL and PsbA after several days in darkness (Figs 1a,d,h, 5).

Features characteristic of quiescence are found in *F. cylindrus* in prolonged darkness (Sun & Gresham, 2021), including the overall drop in metabolic activity, shown by the downregulation

New Phytologist

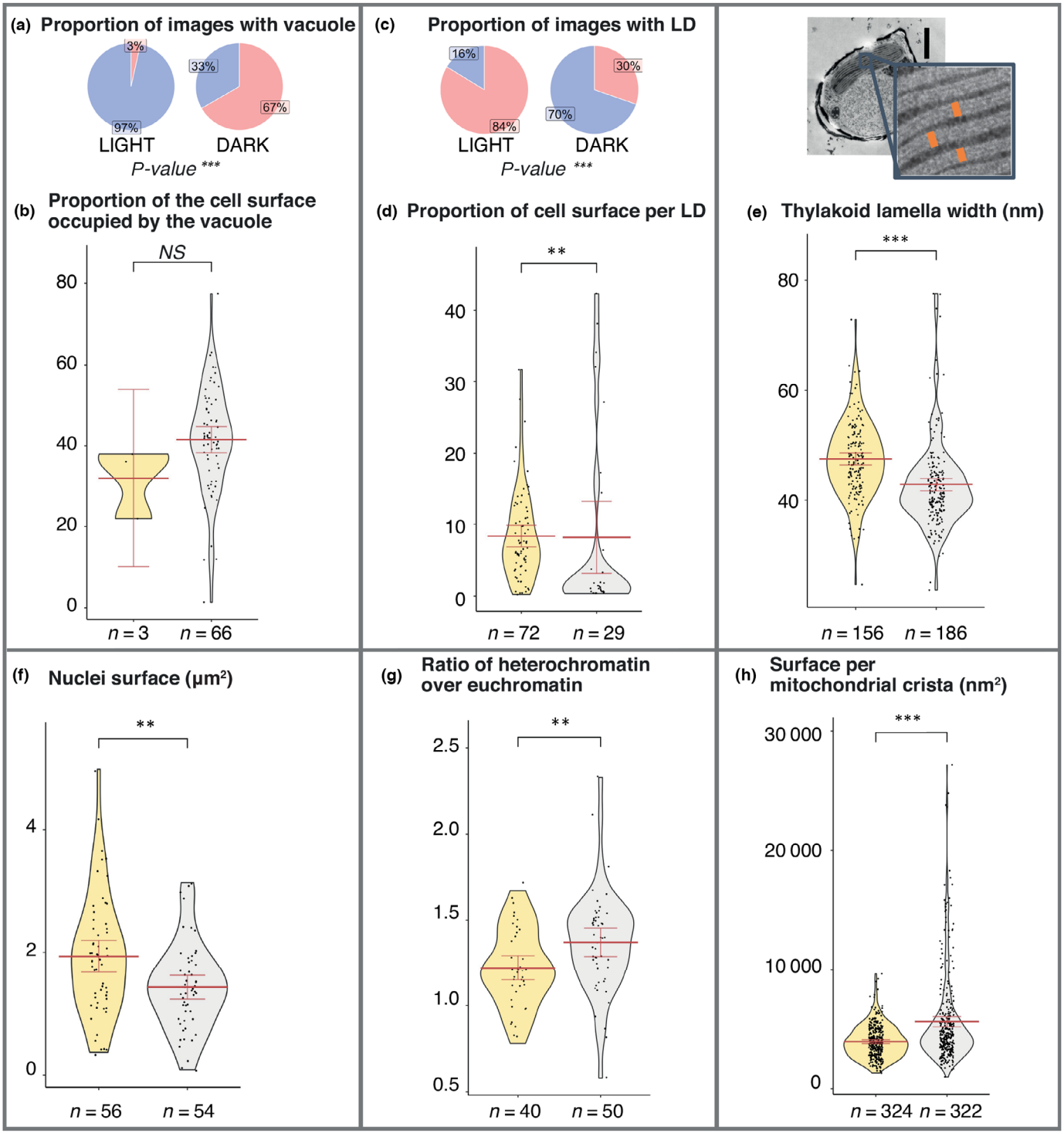

Fig. 3 Analyses of transmission electron microscopy images of *Fragilariopsis cylindrus* cells from continuous light (yellow plots) and after prolonged darkness (grey plots) show distinctive structural features. (a) Diagram comparing the proportion of light and dark cells that do not contain a vacuole (blue) to those that do (red). (b) Violin plot displaying light and dark surface area (in %) of the cell cross-section occupied by the vacuole. (c) Diagram comparing the proportion of light and dark cells that do not contain lipid droplets (LD; blue) to those that do (red). (d) Violin plot depicting light and dark surface area (in %) of the cell cross-section occupied by lipid droplets (LD). (e) Images of a dark cell with a zoom on the thylakoid width measurement. Violin plots display the thylakoid lamellae width (in nm) within chloroplasts. Bar, 500 nm. (f) Violin plot comparing the surface area (in μm^2) of the cell cross-section occupied by the nucleus. (g) Violin plot comparing the heterochromatin: euchromatin ratio of the cells. (h) Violin plot of the surface area (in nm^2) of the cell cross-section occupied by mitochondrial cristae in cells. For all violin plots, the mean is shown by the bold horizontal bar; its 95% confidence interval is between the two error bars. *n* is the number of images used for each plot. Result of mean comparison between light and dark cells is represented by its *P*-value above the plots. ns, not significant; *, $0.01 \leq P < 0.05$; **, $0.001 \leq P < 0.01$; ***, $P < 0.001$.

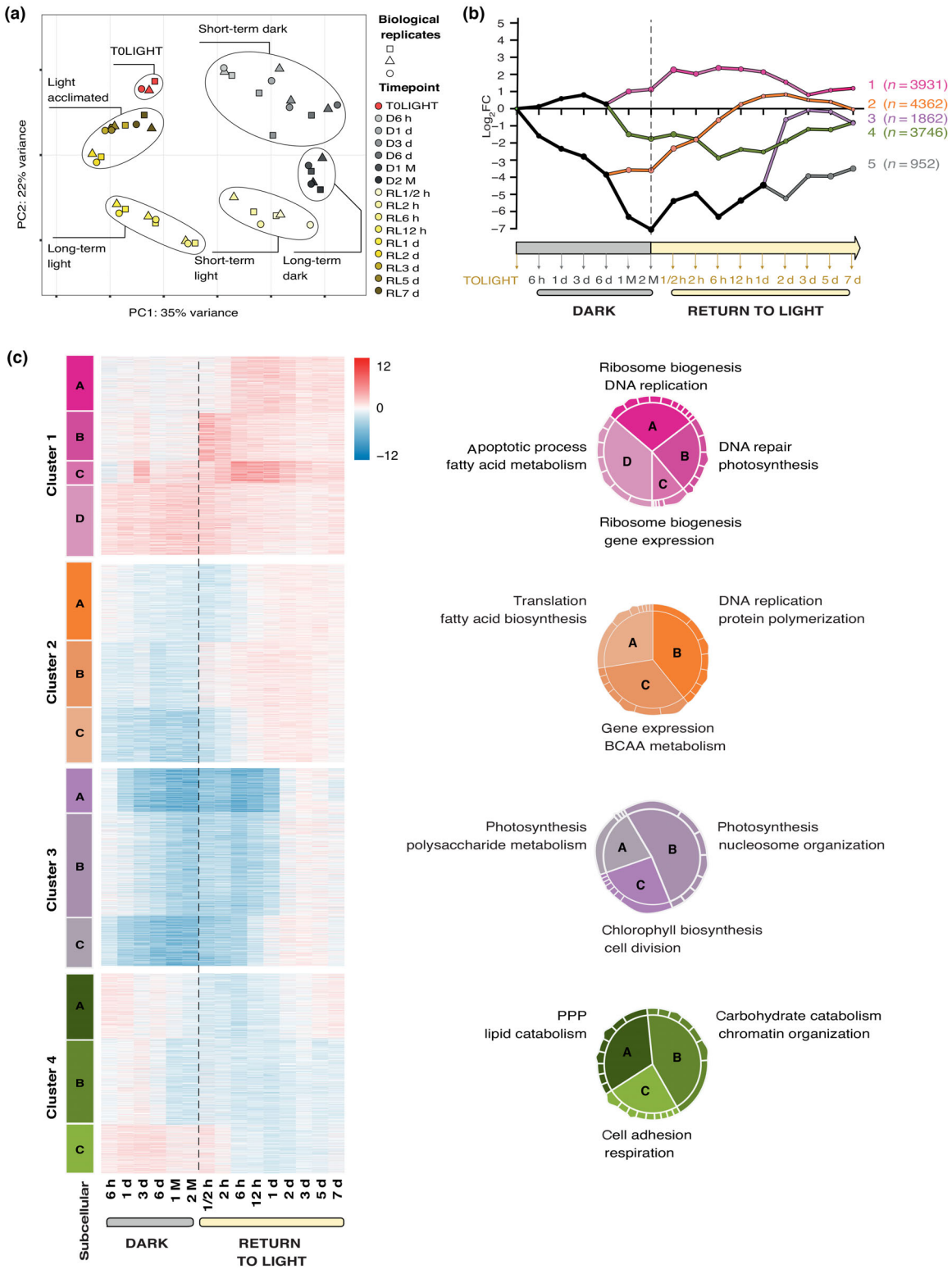

Fig. 4 Gradual transition over time in transcriptomics for functions enriched in cells from cultures of *Fragilariopsis cylindrus* in the acclimation phase in full light (T0LIGHT), in prolonged darkness (from 6 h up to 2 months (M)), and upon return to light (up to 7 d). (a) Principal component analysis of a total of 48 light or dark transcriptomes. Each dot represents one transcriptome and the shapes refer to one of the three biological replicates. (b) Dynamic Regulatory Events Miner analysis using the differentially expressed genes compared with the acclimation phase. The numbers on the right refer to the number of the cluster along with the number of genes within each cluster. (c) Each of the clusters is divided into subclusters illustrated by letters on the left of each heatmap (A to C or A to D). Heatmaps show the average $\log_2$ fold expression ($\log_2$FC) of genes compared to the light-acclimated time point. Pie charts on the right of each heatmap indicate the Gene Ontology (GO) enrichment within each subcluster. Only two GOs per subcluster are shown (notched sectors). The full list of enriched GOs is given in Supporting Information Table S3.

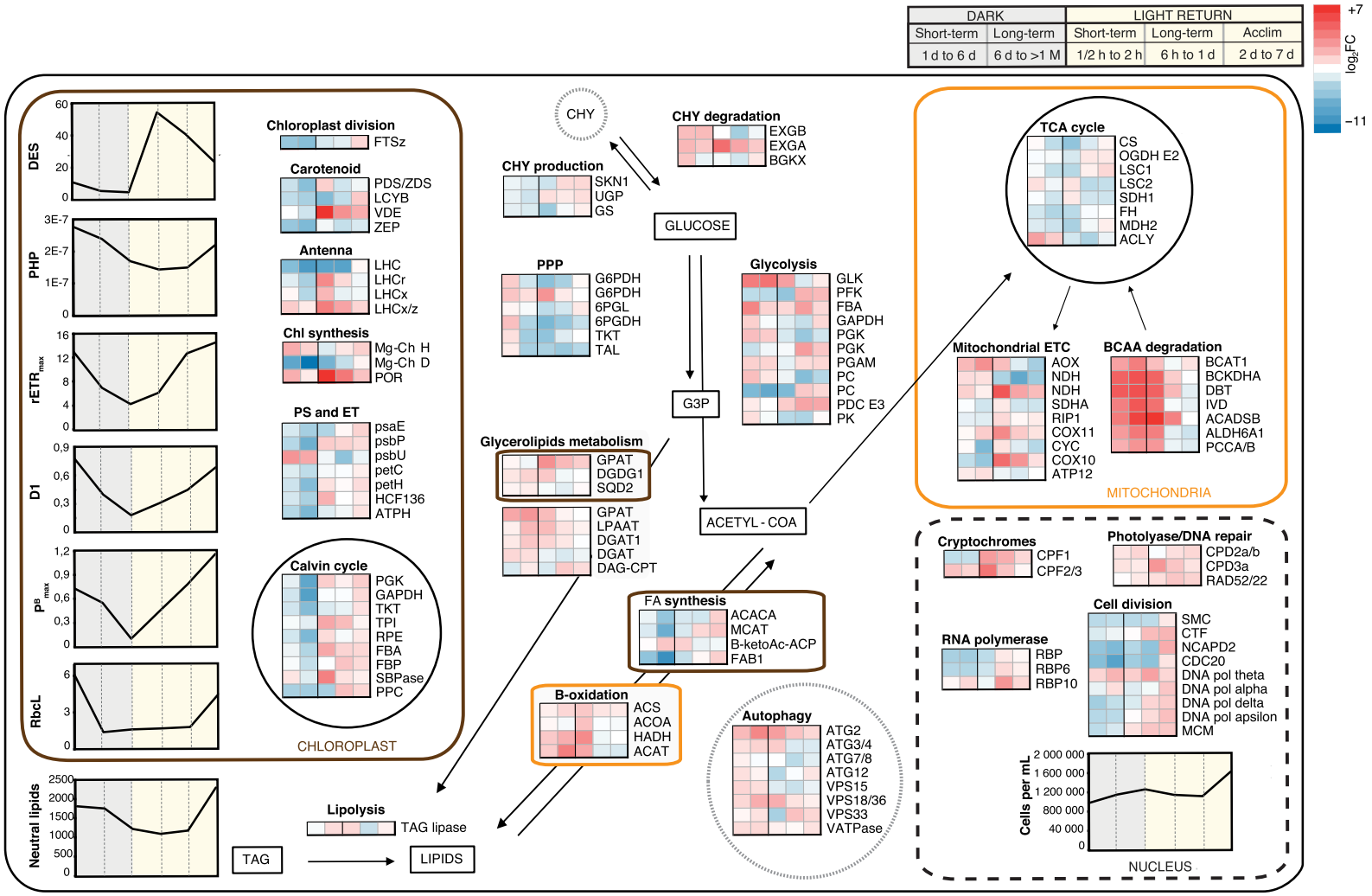

Fig. 5 Cell schematic displaying expression of selected genes of interest in *Fragilariopsis cylindrus*. Colored squares indicate the average $\log_2$ fold expression change ($\log_2$FC) in each time window relative to the pre-dark acclimation phase. Red represents higher expression, and blue represents lower expression. Short-term dark (1–6 d), long-term dark (> 6 d to 2 months (M)), short-term light return (30 min to 2 h), long-term light return (6 h to 1 d) and light acclimation (2–7 d) conditions are represented. Genes involved in metabolic pathways located in the chloroplast are represented inside a brown box, those in the mitochondria inside an orange box. Those in the nucleus are shown inside a black dashed box and those in vacuoles in grey dotted circles. Percentage de-epoxidation state (DES), sum of photosynthetic pigments (PHP = Chl*a* + Chl*c* + Fx) in µg cell^{-1}, maximum relative electron transport rate (rETR$_{max}$), maximum productivity (P^B_{max}), neutral lipids expressed in relative fluorescence units and photosynthetic proteins are represented (RbcL and D1 in µg). $\log_2$FC of genes having the same temporal trend and the same enzyme/function were averaged. The complete list of corresponding gene names with their acronyms, the number of genes considered and the subcellular predictions is given in Supporting Information Table S5. BCAA, branched-chain amino acid; ET, electron transport; ETC, electron transport chain; FA, fatty acid; PPP, pentose phosphate pathway; PS, photosystems; TCA, tricarboxylic acid cycle.

of RNA polymerase II subunit genes (Fig. 5), and by the drastic decrease in the active form of RNA polymerase II protein by immunoblot (Fig. S7). On average, the total protein level per cell drops to 22% (13%) after 1 month in the dark as compared to T0LIGHT (Fig. S2k), consistent with the downregulation of genes involved in ribosome biogenesis (Fig. 4c). As found in quiescent yeast and animals, cell size is slightly reduced in the dark (Fig. S2a; Lacour *et al.*, 2019).

Branched-chain amino acids play a key role in environmental adaptation in diatoms (Yao *et al.*, 2017). We find several genes involved in branched-chain amino acid metabolism that shows strong overexpression relative to T0LIGHT throughout the dark period. Most of the genes involved in fatty acid synthesis are downregulated in the dark while several triacylglycerols lipases and beta oxidation-related genes are induced. The expression profile of genes involved in glycolipid metabolism (digalactosyldiacylglycerol synthase *DGDG1* and sulfoquinovosyltransferase *SQD2*) and in triacylglycerols synthesis (glycerol-3-phosphate acyltransferase *GPAT* and diacylglycerol acyltransferase *DGAT*) along with the decrease of thylakoid lamellae thickness suggest a potential rearrangement or consumption of cellular lipids in prolonged darkness (Figs 3e, 5) in accordance with the TEM analysis (Fig. 3c,d) and with the decrease in the cytometry fluorescence signal of the triacylglycerols stock in lipid droplets (Fig. 5; Tables S5, S6; Rumin *et al.*, 2015; Sciandra *et al.*, 2022). The upregulation of glucosidase genes and the downregulation of chrysolaminarin production genes (Figs 4c, 5) suggest that it is also consumed.

The upregulation of light-harvesting complex *LHCx* and *LHCz* genes in prolonged darkness illustrates that, as in other polar diatoms, capacity for nonphotochemical quenching is a key strategy for energy dissipation upon the abrupt return of light (Figs 5, S2g,h; Lacour *et al.*, 2019). Therefore, photoprotection is induced rapidly after light return and then relaxed as the $rETR_{max}$ and P^{B}_{max} slowly increase to their light-acclimated values after 2–3 d. The immediate increase in $rETR_{max}$ when light returns suggests a re-organization of the existing photosystems rather than *de novo* synthesis (Baldisserotto *et al.*, 2005a; Ferroni *et al.*, 2007; Nymark *et al.*, 2013; Lacour *et al.*, 2019).

Interestingly, the continuous change from the transcriptomic short-term response to light (6 h to 1 d) to longer-term response is consistent with the progressive increase in protein content per cell and in the observed changes in photosynthetic parameters. A return to nearly the initial state of gene expression was observed after 2–3 d of light return, as the cell produces new photosynthetic pigments and divides, in conjunction with upregulation of cell division-related genes (Figs 4a, 5, S2f).

Discussion

We have explored the responses of the polar diatom *F. cylindrus* to an extended period of darkness followed by an acute exposure to light in order to disentangle mechanisms related to survival during the long polar night. Consistent with previous studies, we demonstrate that the majority of the cell population acclimates to prolonged darkness (Wulff *et al.*, 2008; Reeves *et al.*, 2011; Lacour *et al.*, 2019; Morin *et al.*, 2020). We present evidence that the cell enters into a quiescent state (Shemi *et al.*, 2016; Zienkiewicz *et al.*, 2020) and that a toolbox of genes and metabolic pathways are associated with survival in darkness and subsequent successful return to the light.

As observed in other species of microalgae in the dark (Palmisano & Sullivan, 1982; Dehning & Tilzer, 1989; Schaub *et al.*, 2017; Morin *et al.*, 2020), *F. cylindrus* reduced its metabolic activity, consuming little of its energy reserves (Fig. 1f). We propose that induction of autophagy in *F. cylindrus* in prolonged darkness contributes to the degradation of cell reserves, notably fatty acids, which provide essential elements for the cell to ensure energy homeostasis. Autophagy can lead to programmed cell death under severe stress but it is also involved in the degradation of lipid droplets in microalgae, sometimes through their uptake into vacuoles (Zhao *et al.*, 2014; Shemi *et al.*, 2015; Zienkiewicz *et al.*, 2020), known as lipophagy in quiescent yeast (Wang *et al.*, 2014). Given the increased expression of genes encoding the central components of autophagy (autophagy-related protein ATG and the vacuolar sorting protein VPS) and genes associated with apoptosis (Figs 4, 5, S6) during this period, we propose that vacuole-mediated autophagy is initiated after 3 d of darkness and may be a means of avoiding accumulation of harmful waste products in the cytoplasm. Vacuolar features similar to the large vacuole appearing here have been observed in *P. tricornutum*, in Antarctic red algae, in chlorophytes and in *Emiliania huxleyi*. It may support material digestion of cell constituents in the dark or in nutrient-depleted environment (Ferroni *et al.*, 2007; Nymark *et al.*, 2013; Shemi *et al.*, 2015, 2016). Of note, two TEM pictures suggest the presence of material inside the vacuoles in the dark that may represent cellular material being recycled (Fig. S3d).

Although counterintuitive because this metabolic pathway produces less ATP compared with the cytochrome oxidase (COX) pathway, *F. cylindrus* upregulates the AOX-dependent respiration pathway genes (complexes I and II of the mitochondrial electron transport chain (AOX, NADH dehydrogenase (*NDH*), succinate dehydrogenase (*SDHA*)) in prolonged darkness. A previous study showed undetectable ATP levels in prolonged darkness in *F. cylindrus* but also found that AOX partner proteins were upregulated (Kennedy *et al.*, 2019). This suggests that the AOX pathway, which can play a role in cellular adaptation under different types of stress (Bailleul *et al.*, 2015; Murik *et al.*, 2019), is also operational in the dark. Conversely, COX-associated genes (mitochondrial complex III, ubiquinol cytochrome c reductase (*RIP1*)) are relatively more strongly induced immediately following the return to light (Figs 4, 5, S6). The low rates of respiration in the dark, at least partly through AOX, could help to restrict production of reactive oxygen species (Murik *et al.*, 2019), evocative of the case of quiescent yeast (Allen *et al.*, 2006). Maintaining low reactive oxygen species is essential as it can damage DNA and cellular macromolecules (Gangloff & Arcangioli, 2017).

We also explored the possibility of the involvement of the dark nitrate respiration metabolic pathway described in Kamp *et al.* (2011). Only genes encoding one of the key functions were upregulated in the dark, but was further upregulated following light return as compared to T0LIGHT (Table S6). Because this metabolic pathway is believed to occur in the absence of oxygen,

we therefore conclude it is unlikely to be involved in the dark survival of *F. cylindrus*.

The maintenance of a high photochemical efficiency of PSII F_V/F_M, along with a slight decrease in the effective absorption cross-section σPSII (Figs 1b, S2h,i), indicates a remarkable conservation of the ability to convert light energy by photochemistry throughout the prolonged period of darkness (Nymark *et al.*, 2013; Lacour *et al.*, 2019; Morin *et al.*, 2020). However, photophysiology and carbon fixation were downregulated in the dark in line with numerous studies in other species of both diatoms and other groups of phytoplankton (Dehning & Tilzer, 1989; Peters & Thomas, 1996; Popels *et al.*, 2007; Wulff *et al.*, 2008; Reeves *et al.*, 2011; Lacour *et al.*, 2019). Our results are supported both by measurements at the photochemical and carbon fixation levels, but also at the structural level of the photosynthetic apparatus (Baldisserotto *et al.*, 2005a,b; Ferroni *et al.*, 2007) with a decrease in thylakoid width in prolonged darkness observed by microscopy. Like the few studies that have documented the return to light after a long period of darkness (Peters & Thomas, 1996; Popels *et al.*, 2007; Martin *et al.*, 2012; Lacour *et al.*, 2019; Morin *et al.*, 2020), we observed that *F. cylindrus* restores its photophysiological capacities very quickly (< 1 d) after the return to light and consequently its carbon and nitrogen content (< 2 d; Figs 1, S2). We suggest that the transient drop in F_V/F_M upon the early return of light is related to the activation of photoprotection mechanisms rather than to light-stress-related photodamage of PSII. Of note, the peak in respiration is consistent with the peak in primary production 1 d after return to the light (Fig. 1g,h). The observation that P^B_{max} fell to zero after 2 months of darkness, while $rETR_{max}$ did not, suggests that some capacity for PSII activity is retained during prolonged darkness. The residual PSII ETR may be associated with cyclic electron transport around PSII (Wagner *et al.*, 2016).

Several previous experiments in microalgae suggest a decrease in chlorophyll *a* content per cell in the dark. Here, we found that the chlorophyll *a* pool per cell decreased and also that most of the genes involved in chlorophyll synthesis were downregulated (Table S6; Fig. S2f), suggesting the absence of chlorophyll synthesis in the polar night in *F. cylindrus*. Contrasting with this general trend, two genes encoding enzymes acting in the last steps of chlorophyll synthesis (the magnesium chelatase H subunit and one protochlorophyllide oxidoreductase (POR)) were upregulated in darkness. In plants, angiosperms also require light for chlorophyll synthesis as protochlorophyllide reduction is mediated by light-dependent POR enzymes (PORA, PORB and PORC in *Arabidopsis thaliana*). *PORA* and *PORB* transcripts accumulate to high levels in dark-grown seedlings, conditioning etiolated tissues for rapid greening upon exposure to light, while later in development *PORB* and *PORC* maintain chlorophyll synthesis (Masuda & Takamiya, 2004). The *P. tricornutum* genome encodes two light-dependent POR; POR1, which plays a role during periods of environmental stress and POR2 which supports daily chlorophyll synthesis (Hunsperger *et al.*, 2016). The *F. cylindrus* genome contains several *POR* genes, one of which appears to be strongly induced in response to darkness and the early return of light (Table S6). This not only supports the hypothesis that duplication of *POR* genes in microalgae compensates for the loss of light-independent POR (Hunsperger *et al.*, 2016), but also suggests that this polar diatom accumulates transcripts of this gene during the polar night in order to rapidly convert protochlorophyllide into chlorophyll when light returns (Cvetkovska *et al.*, 2019). Concerning the magnesium chelatase H, this protein has been shown to play a role in chloroplast-to-nucleus retrograde signalling in addition to its role in chlorophyll synthesis, and the high expression of this gene after prolonged darkness could be related to this important regulatory function (Fig. 5; Table S6; Brzezowski *et al.*, 2016; Rea *et al.*, 2018).

We also observed the pre-emptive dark induction of genes in anticipation of the light return involved in photoprotection (*LHCx* and *LHCz* genes) and in DNA repair (encoding cryptochromes CPF2 and 3, CPD photolyase DNA repair and RAD family DNA repair components; Fig. 5). To remain viable, cells must be able to retain DNA integrity, notably DNA repair genes are maintained during hibernation in tardigrades and mammals (Schwartz *et al.*, 2013; Carrero *et al.*, 2019).

After 3 months of total darkness, an acute switch to continuous light at an intensity of 30 µmol photon m^{-2} s^{-1} was designed to simulate an abrupt break-up of sea ice. We believe that similar results would have been obtained even by applying a lower return light level since phytoplankton growth is possible under ice at extremely low light intensities (Randelhoff *et al.*, 2020). Transcriptomic results from another set of samples that spent a month in the dark (Fig. S8) reveal a similar delay in returning to a state of continuous light acclimation, after 7 d of return to light. This illustrates the ability of polar diatoms to withstand the varying durations of polar night experienced across latitudinal gradients. Furthermore, the presence of numerous metabarcoding sequences in several *Tara* Oceans stations corresponding to the genus *Fragilariopsis* above 72°N, where dark conditions over 80 d are encountered in the Arctic in winter (Ludvigsen *et al.*, 2018), supports the environmental relevance of this species as a model of dark adaptation (Fig. S1). Given previous results from studies in nonpolar microalgae species, we cannot exclude the fact that this persistence in prolonged darkness may be a general feature of all microalgae. No other studies in conditions of such prolonged darkness and subsequent return to light have been performed with other species. We suspect, however, that polar species are more likely to succeed in conditions of prolonged darkness and low temperatures (Lacour *et al.*, 2017; Salazar *et al.*, 2019).

Understanding the biology of photosynthetic organisms living in the polar regions and their tolerance to environmental changes is now of pressing importance, as they evolve towards warmer temperatures while still enduring extreme variations in seasonal light. Although some experiments conducted on polar algae indicate that survival rates in the dark are not affected by moderate temperature increases (Reeves *et al.*, 2011; Martin *et al.*, 2012), we nevertheless expect shorter dark survival times with increasing water temperatures, given the higher temperature-dependent metabolic rates (Schaub *et al.*, 2017).

Several of our results are innovative, suggesting strategies on how a model polar diatom, survives and exits the dark polar winter. The long-term dark survival strategy of *F. cylindrus* involves a

slow-down of metabolism and the establishment of a specific and reversible gene expression programme for dark survival. We observed a modification of the subcellular organization, and we propose that the cell uses an autophagic compartment to degrade cellular compounds. The AOX pathway potentially plays an important role in enabling the cell to respire at lower rates, thus causing less oxidative damage to the cell, but it may also contribute to maintaining cellular bioenergetic processes at a rate such that they do not burn up energy reserves too quickly. Despite this suppressed physiological state, the polar diatom adopts a 'better prevent than cure' strategy maintaining the expression of genes in the dark involved in chlorophyll production, photoprotection and DNA repair and retains its ability to rapidly reset growth following the return of light. Further experiments could be carried out using advanced genetic manipulation techniques or pharmacological inhibitors specific to target genes or pathways. Inhibiting the AOX pathway could help elucidate how organisms cope with accumulation of cell-damaging waste products during periods of darkness. Inhibition of autophagy-related genes may enable to determine whether autophagy is essential for entry into a quiescent state and long-term survival in the dark. Finally, to go beyond the measurement of relative transcript abundance and achieve absolute quantification of dark vs light transcripts, it would be highly recommended to use a method such as RNA-Seq spike-in Quinn *et al.* (2018).

Acknowledgements

We acknowledge the contributions of all the staff who participated in the multiple sampling events. We thank Leila Tirichine for her contribution in the early stages of this project and Fredy Barneche for his continuous support. We thank Natalie Donaher for analysing protein data and Gabrièle Deslongchamps for the nutrient data. We thank the IBENS imaging facility (IMACHEM-IBiSA) for their help in generating the confocal microscopy images. We also thank Florian Maumus for the detection of the transposable elements. Finally, we thank the EMBL Electron Microscopy Core Facility for their assistance in generating electron microscopy data. This work was supported by the HFSP project Green Life in the Dark (grant RGP0003/2016) to MB and ChB. This project has also received funding from the European Research Council (ERC) under the European Union's Horizon 2020 research and innovation programme (Diatomic; grant agreement no. 835067). This work was further Funded by the Sentinel North programme of Université Laval (Canada First Research Excellence Fund), by the Canada Excellence Research Chair on Remote sensing of Canada's new Arctic frontier and by NSERC Discovery grants to MB and DAC.

Competing interests

None declared.

Author contributions

MB and C Bowler designed the research. NJ, KM, J Laude, SG, TS, FB, Marine Beguin, MHF, MS and JET collected the data. NJ, LC, KM, JG, J Laude, SG, FB, OAM, C Bourbousse, CN, MS, JET and J Lavaud analysed the data. NJ involved in writing – original draft. All co-authors involved in writing – review and editing. LC and KM contributed equally to this work. JG and J Laude contributed equally to this work.

ORCID

Ouardia Ait-Mohamed https://orcid.org/0000-0002-7637-6958
Marcel Babin https://orcid.org/0000-0001-9233-2253
Clara Bourbousse https://orcid.org/0000-0001-6464-6124
Chris Bowler https://orcid.org/0000-0003-3835-6187
Flavienne Bruyant https://orcid.org/0000-0003-4155-4811
Lorenzo Concia https://orcid.org/0000-0002-7401-7214
Marie-Helene Forget https://orcid.org/0000-0002-2430-8531
Sebastien Guerin https://orcid.org/0000-0002-3243-7755
Nathalie Joli https://orcid.org/0000-0002-3832-8066
Thomas Lacour https://orcid.org/0000-0003-2295-6188
Juliette Laude https://orcid.org/0000-0001-7363-1194
Johann Lavaud https://orcid.org/0000-0002-4704-2502
Karel Mocaer https://orcid.org/0000-0002-9706-6457
Charlotte Nef https://orcid.org/0000-0002-9446-6367
Yannick Schwab https://orcid.org/0000-0001-8027-1836
Theo Sciandra https://orcid.org/0000-0001-6938-6253
Jean-Eric Tremblay https://orcid.org/0000-0003-0319-5723

Data availability

All data are available in the main text or the Supporting Information.

References

Allen C, Büttner S, Aragon AD, Thomas JA, Meirelles O, Jaetao JE, Benn D, Ruby SW, Veenhuis M, Madeo F *et al.* 2006. Isolation of quiescent and nonquiescent cells from yeast stationary-phase cultures. *Journal of Cell Biology* **174**: 89–100.

Bailleul B, Berne N, Murik O, Petroutsos D, Prihoda J, Tanaka A, Villanova V, Bligny R, Flori S, Falconet D *et al.* 2015. Energetic coupling between plastids and mitochondria drives CO_2 assimilation in diatoms. *Nature* **524**: 366–369.

Baldisserotto C, Ferroni L, Andreoli C, Fasulo MP, Bonora A, Pancaldi S. 2005a. Dark-acclimation of the chloroplast in *Koliella Antarctica* exposed to a simulated austral night condition. *Arctic, Antarctic, and Alpine Research* **37**: 146–156.

Baldisserotto C, Ferroni L, Moro I, Fasulo MP, Pancaldi S. 2005b. Modulations of the thylakoid system in snow xanthophycean alga cultured in the dark for two months: comparison between microspectrofluorimetric responses and morphological aspects. *Protoplasma* **226**: 125–135.

Barnett A, Méléder V, Blommaert L, Lepetit B, Gaudin P, Vyverman W, Sabbe K, Dupuy C, Lavaud J. 2015. Growth form defines physiological photoprotective capacity in intertidal benthic diatoms. *The ISME Journal* **9**: 32–45.

Blix AS. 2016. Adaptations to polar life in mammals and birds. *Journal of Experimental Biology* **219**: 1093–1105.

Bowler C, Vardi A, Allen AE. 2010. Oceanographic and biogeochemical insights from diatom genomes. *Annual Review of Marine Science* **2**: 333–365.

Brzezowski P, Sharifi MN, Dent RM, Morhard MK, Niyogi KK, Grimm B. 2016. Mg chelatase in chlorophyll synthesis and retrograde signaling in

Chlamydomonas reinhardtii: CHLI2 cannot substitute for CHLI1. *Journal of Experimental Botany* **67**: 3925–3938.

Carrero D, Pérez-Silva JG, Quesada V, López-Otín C. 2019. Differential mechanisms of tolerance to extreme environmental conditions in tardigrades. *Scientific Reports* **9**: 14938.

Cherkezyan L, Stypula-Cyrus Y, Subramanian H, White C, Dela Cruz M, Wali RK, Goldberg MJ, Bianchi LK, Roy HK, Backman V. 2014. Nanoscale changes in chromatin organization represent the initial steps of tumorigenesis: a transmission electron microscopy study. *BMC Cancer* **14**: 189.

Chiovitti A, Molino P, Crawford SA, Teng R, Spurck T, Wetherbee R. 2004. The glucans extracted with warm water from diatoms are mainly derived from intracellular chrysolaminaran and not extracellular polysaccharides. *European Journal of Phycology* **39**: 117–128.

Coesel S, Mangogna M, Ishikawa T, Heijde M, Rogato A, Finazzi G, Todo T, Bowler C, Falciatore A. 2009. Diatom PtCPF1 is a new cryptochrome/photolyase family member with DNA repair and transcription regulation activity. *EMBO Reports* **10**: 655–661.

Croteau D, Guérin S, Bruyant F, Ferland J, Campbell DA, Babin M, Lavaud J. 2021. Contrasting nonphotochemical quenching patterns under high light and darkness aligns with light niche occupancy in Arctic diatoms. *Limnology and Oceanography* **66**: S231–S245.

Croteau D, Lacour T, Schiffrine N, Morin P, Forget M, Bruyant F, Ferland J, Lafond A, Campbell DA, Tremblay J *et al.* 2022. Shifts in growth light optima among diatom species support their succession during the spring bloom in the Arctic. *Journal of Ecology* **110**: 1356–1375.

Cvetkovska M, Orgnero S, Hüner NPA, Smith DR. 2019. The enigmatic loss of light-independent chlorophyll biosynthesis from an Antarctic green alga in a light-limited environment. *New Phytologist* **222**: 651–656.

Dehning I, Tilzer MM. 1989. Survival of *Scenedescmus acuminatus* (Chlorophyceae) in darkness. *Journal of Phycology* **25**: 509–515.

Eilers PHC, Peeters JCH. 1988. A model for the relationship between light intensity and the rate of photosynthesis in phytoplankton. *Ecological Modelling* **42**: 199–215.

Falciatore A, Bailleul B, Boulouis A, Bouly J-P, Bujaldon S, Cheminant-Navarro S, Choquet Y, De Vitry C, Eberhard S, Jaubert M *et al.* 2022. Light-driven processes: key players of the functional biodiversity in microalgae. *Comptes Rendus. Biologies* **345**: 15–38.

Ferroni L, Baldisserotto C, Zennaro V, Soldani C, Fasulo MP, Pancaldi S. 2007. Acclimation to darkness in the marine chlorophyte *Koliella antarctica* cultured under low salinity: Hypotheses on its origin in the polar environment. *European Journal of Phycology* **42**: 91–104.

Field CB, Behrenfeld MJ, Randerson JT, Falkowski P. 1998. Primary production of the biosphere: integrating terrestrial and oceanic components. *Science* **281**: 237–240.

Flutre T, Duprat E, Feuillet C, Quesneville H. 2011. Considering transposable element diversification in *de novo* annotation approaches. *PLoS ONE* **6**: e16526.

Gangloff S, Arcangioli B. 2017. DNA repair and mutations during quiescence in yeast. *FEMS Yeast Research* **17**: fox002.

Goss R, Lepetit B. 2015. Biodiversity of NPQ. *Journal of Plant Physiology* **172**: 13–32.

Griffiths DJ. 1973. Factors affecting the photosynthetic capacity of laboratory cultures of the diatom *Phaeodactylum tricornutum*. *Marine Biology* **21**: 91–97.

Handa N. 1969. Carbohydrate metabolism in the marine diatom *Skeletonema costatum*. *Marine Biology* **4**: 208–214.

Hellebust JA, Terborgh J. 1967. Effect of environmental conditions on the rate of photosynthesis and some photosynthetic enzymes in *Dunaliella tertiolecta butcher*: environmental effect on photosynthetic. *Limnology and Oceanography* **12**: 559–567.

Hennies J, Lleti JMS, Schieber NL, Templin RM, Steyer AM, Schwab Y. 2020. AMST: alignment to median smoothed template for focused ion beam scanning electron microscopy image stacks. *Scientific Reports* **10**: 2004.

Hoban MA, Fryxell GA, Buck KR. 1980. Ciddulphioid diatoms: resting spores in Antarctic Eucampia and Odontella. *Journal of Phycology* **16**: 591–602.

Hunsperger HM, Ford CJ, Miller JS, Cattolico RA. 2016. Differential regulation of duplicate light-dependent protochlorophyllide oxidoreductases in the diatom *Phaeodactylum tricornutum*. *PLoS ONE* **11**: e0158614.

Ibarbalz FM, Henry N, Brandão MC, Martini S, Busseni G, Byrne H, Coelho LP, Endo H, Gasol JM, Gregory AC *et al.* 2019. Global trends in marine plankton diversity across kingdoms of life. *Cell* **179**: 1084–1097.

Kamp A, De Beer D, Nitsch JL, Lavik G, Stief P. 2011. Diatoms respire nitrate to survive dark and anoxic conditions. *Proceedings of the National Academy of Sciences, USA* **108**: 5649–5654.

Kennedy F, Martin A, Bowman JP, Wilson R, McMinn A. 2019. Dark metabolism: a molecular insight into how the Antarctic sea-ice diatom *Fragilariopsis cylindrus* survives long-term darkness. *New Phytologist* **223**: 675–691.

Kolber ZS, Prášil O, Falkowski PG. 1998. Measurements of variable chlorophyll fluorescence using fast repetition rate techniques: defining methodology and experimental protocols. *Biochimica et Biophysica Acta (BBA) – Bioenergetics* **1367**: 88–106.

Kuwata A, Hama T, Takahashi M. 1993. Ecophysiological characterization of two life forms, resting spores and resting cells, of a marine planktonic diatom, *Chaetoceros pseudocurvisetus*, formed under nutrient depletion. *Marine Ecology Progress Series* **102**: 245–255.

Lacour T, Larivière J, Babin M. 2017. Growth, Chl *a* content, photosynthesis, and elemental composition in polar and temperate microalgae. *Limnology and Oceanography* **62**: 43–58.

Lacour T, Larivière J, Ferland J, Bruyant F, Lavaud J, Babin M. 2018. The role of sustained photoprotective non-photochemical quenching in low temperature and high light acclimation in the bloom-forming arctic diatom *Thalassiosira gravida*. *Frontiers in Marine Science* **5**: 354.

Lacour T, Morin PI, Sciandra T, Donaher N, Campbell DA, Ferland J, Babin M. 2019. Decoupling light harvesting, electron transport and carbon fixation during prolonged darkness supports rapid recovery upon re-illumination in the Arctic diatom *Chaetoceros neogracilis*. *Polar Biology* **42**: 1787–1799.

Lin X, Tirichine L, Bowler C. 2012. Protocol: chromatin immunoprecipitation (ChIP) methodology to investigate histone modifications in two model diatom species. *Plant Methods* **8**: 1–9.

Lüder UH, Wiencke C, Knoetzel J. 2002. Acclimation of photosynthesis and pigments during and after six months of darkness in *Palmaria decipiens* (Rhodophyta): a study to simulate Antarctic winter sea ice cover. *Journal of Phycology* **38**: 904–913.

Ludvigsen M, Berge J, Geoffroy M, Cohen JH, De La Torre PR, Nornes SM, Singh H, Sørensen AJ, Daase M, Johnsen G. 2018. Use of an Autonomous Surface Vehicle reveals small-scale diel vertical migrations of zooplankton and susceptibility to light pollution under low solar irradiance. *Science Advances* **4**: eaap9887.

Ma L, Li J, Qu L, Hager J, Chen Z, Zhao H, Deng XW. 2001. Light control of Arabidopsis development entails coordinated regulation of genome expression and cellular pathways. *Plant Cell* **13**: 2589–2607.

Malviya S, Scalco E, Audic S, Vincent F, Veluchamy A, Poulain J, Wincker P, Iudicone D, de Vargas C, Bittner L *et al.* 2016. Insights into global diatom distribution and diversity in the world's ocean. *Proceedings of the National Academy of Sciences, USA* **113**: E1516–E1525.

Martin A, McMinn A, Heath M, Hegseth EN, Ryan KG. 2012. The physiological response to increased temperature in over-wintering sea ice algae and phytoplankton in McMurdo Sound, Antarctica and Tromsø Sound, Norway. *Journal of Experimental Marine Biology and Ecology* **428**: 57–66.

Masuda T, Takamiya K. 2004. Novel insights into the enzymology, regulation and physiological functions of light-dependent protochlorophyllide oxidoreductase in angiosperms. *Photosynthesis Research* **81**: 1–29.

McMinn A, Martin A. 2013. Dark survival in a warming world. *Proceedings of the Royal Society B: Biological Sciences* **280**: 1–7.

McQuoid MR, Hobson LA. 1996. Diatom resting stages. *Journal of Phycology* **32**: 889–902.

Mock T, Otillar RP, Strauss J, McMullan M, Paajanen P, Schmutz J, Salamov A, Sanges R, Toseland A, Ward BJ *et al.* 2017. Evolutionary genomics of the cold-adapted diatom *Fragilariopsis cylindrus*. *Nature* **541**: 536–540.

Montanaro J, Gruber D, Leisch N. 2016. Improved ultrastructure of marine invertebrates using non-toxic buffers. *PeerJ* **4**: e1860.

Morel FMM, Rueter JG, Anderson DM, Guillard RRL. 1979. AQUIL: a chemically defined phytoplankton culture medium for trace metal studies. *Journal of Phycology* **15**: 135–141.

Morin PI, Lacour T, Grondin PL, Bruyant F, Ferland J, Forget MH, Massicotte P, Donaher N, Campbell DA, Lavaud J *et al.* 2020. Response of the sea-ice diatom *Fragilariopsis cylindrus* to simulated polar night darkness and return to light. *Limnology and Oceanography* **65**: 1041–1060.

Moriya Y, Itoh M, Okuda S, Yoshizawa AC, Kanehisa M. 2007. KAAS: an automatic genome annotation and pathway reconstruction server. *Nucleic Acids Research* **35**: W182–W185.

Murik O, Tirichine L, Prihoda J, Thomas Y, Araújo WL, Allen AE, Fernie AR, Bowler C. 2019. Downregulation of mitochondrial alternative oxidase affects chloroplast function, redox status and stress response in a marine diatom. *New Phytologist* **221**: 1303–1316.

Nymark M, Valle KC, Hancke K, Winge P, Andresen K, Johnsen G, Bones AM, Brembu T. 2013. Molecular and photosynthetic responses to prolonged darkness and subsequent acclimation to re-Illumination in the diatom *Phaeodactylum tricornutum*. *PLoS ONE* **8**: e58722.

Olaizola M, La Roche J, Kolber Z, Falkowski PG. 1994. Non-photochemical fluorescence quenching and the diadinoxanthin cycle in a marine diatom. *Photosynthesis Research* **41**: 357–370.

Palmisano AC, Sullivan CW. 1982. Physiology of sea ice diatoms. I. Response of three polar diatoms to a simulated summer-winter transition. *Journal of Phycology* **18**: 489–498.

Palmisano AC, Sullivan CW. 1983. Sea ice microbial communities (SIMCO): 1. Distribution, abundance, and primary production of ice microalgae in McMurdo Sound, Antarctica in 1980. *Polar Biology* **2**: 171–177.

Peters E, Thomas DN. 1996. Prolonged darkness and diatom mortality I: Marine Antarctic species. *Journal of Experimental Marine Biology and Ecology* **207**: 25–41.

Pierella Karlusich JJ, Ibarbalz FM, Bowler C. 2020. Phytoplankton in the *Tara* Ocean. *Annual Review of Marine Science* **12**: 233–265.

Platt T, Gallegos C, Harrison W. 1981. Photoinhibition of photosynthesis in natural assemblages of marine phytoplankton. *Journal of Marine Research* **38**: 687–701.

Popels LC, MacIntyre HL, Warner ME, Zhang Y, Hutchins DA. 2007. Physiological responses during dark survival and recovery in *Aureococcus anophagefferens* (Pelagophyceae). *Journal of Phycology* **43**: 32–42.

Quesneville H, Bergman CM, Andrieu O, Autard D, Nouaud D, Ashburner M, Anxolabehere D. 2005. Combined evidence annotation of transposable elements in genome sequences. *PLoS Computational Biology* **1**: 166–175.

Quinn TP, Erb I, Richardson MF, Crowley TM. 2018. Understanding sequencing data as compositions: an outlook and review. *Bioinformatics* **34**: 2870–2878.

Randelhoff A, Lacour L, Marec C, Leymarie E, Lagunas J, Xing X, Darnis G, Penkerc'h C, Sampei M, Fortier L *et al.* 2020. Arctic mid-winter phytoplankton growth revealed by autonomous profilers. *Science Advances* **6**: eabc2678.

Ras J, Claustre H, Uitz J. 2008. Spatial variability of phytoplankton pigment distributions in the Subtropical South Pacific Ocean: comparison between *in situ* and predicted data. *Biogeosciences* **5**: 353–369.

Rea G, Antonacci A, Lambreva MD, Mattoo AK. 2018. Features of cues and processes during chloroplast-mediated retrograde signaling in the alga Chlamydomonas. *Plant Science* **272**: 193–206.

Reeves S, McMinn A, Martin A. 2011. The effect of prolonged darkness on the growth, recovery and survival of Antarctic sea ice diatoms. *Polar Biology* **34**: 1019–1032.

Ronchi P, Mizzon G, Machado P, D'Imprima E, Best BT, Cassella L, Schnorrenberg S, Montero MG, Jechlinger M, Ephrussi A *et al.* 2021. High-precision targeting workflow for volume electron microscopy. *Journal of Cell Biology* **220**: e202104069.

Rumin J, Bonnefond H, Saint-Jean B, Rouxel C, Sciandra A, Bernard O, Cadoret J-P, Bougaran G. 2015. The use of fluorescent Nile red and BODIPY for lipid measurement in microalgae. *Biotechnology for Biofuels* **8**: 42.

Salazar G, Paoli L, Alberti A, Huerta-Cepas J, Ruscheweyh HJ, Cuenca M, Field CM, Coelho LP, Cruaud C, Engelen S *et al.* 2019. Gene expression changes and community turnover differentially shape the global ocean metatranscriptome. *Cell* **179**: 1068–1083.

Schaub I, Wagner H, Graeve M, Karsten U. 2017. Effects of prolonged darkness and temperature on the lipid metabolism in the benthic diatom *Navicula perminuta* from the Arctic Adventfjorden, Svalbard. *Polar Biology* **40**: 1425–1439.

Schulz MH, Devanny WE, Gitter A, Zhong S, Ernst J, Bar-Joseph Z. 2012. DREM 2.0: improved reconstruction of dynamic regulatory networks from time-series expression data. *BMC Systems Biology* **6**: 104.

Schwartz C, Hampton M, Andrews MT. 2013. Seasonal and regional differences in gene expression in the brain of a hibernating mammal. *PLoS ONE* **8**: e58427.

Sciandra T, Forget M, Bruyant F, Béguin M, Lacour T, Bowler C, Babin M. 2022. The possible fates of *Fragilariopsis cylindrus* (polar diatom) cells exposed to prolonged darkness. *Journal of Phycology* **58**: 281–296.

Serôdio J, Lavaud J. 2011. A model for describing the light response of the nonphotochemical quenching of chlorophyll fluorescence. *Photosynthesis Research* **108**: 61–76.

Shemi A, Ben-Dor S, Vardi A. 2015. Elucidating the composition and conservation of the autophagy pathway in photosynthetic eukaryotes. *Autophagy* **11**: 701–715.

Shemi A, Schatz D, Fredricks HF, Van Mooy BAS, Porat Z, Vardi A. 2016. Phosphorus starvation induces membrane remodeling and recycling in *Emiliania huxleyi*. *New Phytologist* **211**: 886–898.

Storey KB, Storey JM. 2007. Tribute to P. L. Lutz: putting life on 'pause' – molecular regulation of hypometabolism. *Journal of Experimental Biology* **210**: 1700–1714.

Sun S, Gresham D. 2021. Cellular quiescence in budding yeast. *Yeast* **38**: 12–29.

Tréguer PJ, Sutton JN, Brzezinski M, Charette MA, Devries T, Dutkiewicz S, Ehlert C, Hawkings J, Leynaert A, Liu SM *et al.* 2021. Reviews and syntheses: the biogeochemical cycle of silicon in the modern ocean. *Biogeosciences* **18**: 1269–1289.

Wagner H, Jakob T, Lavaud J, Wilhelm C. 2016. Photosystem II cycle activity and alternative electron transport in the diatom *Phaeodactylum tricornutum* under dynamic light conditions and nitrogen limitation. *Photosynthesis Research* **128**: 151–161.

Wang C-W, Miao Y-H, Chang Y-S. 2014. A sterol-enriched vacuolar microdomain mediates stationary phase lipophagy in budding yeast. *Journal of Cell Biology* **206**: 357–366.

Wulff A, Roleda MY, Zacher K, Wiencke C. 2008. Exposure to sudden light burst after prolonged darkness – a case study on benthic diatoms in Antarctica. *Diatom Research* **23**: 519–532.

Yao L, Shen H, Wang N, Tatlay J, Li L, Tan TW, Lee YK. 2017. Elevated acetyl-CoA by amino acid recycling fuels microalgal neutral lipid accumulation in exponential growth phase for biofuel production. *Plant Biotechnology Journal* **15**: 497–509.

Zhao L, Dai J, Wu Q. 2014. Autophagy-like processes are involved in lipid droplet degradation in *Auxenochlorella protothecoides* during the heterotrophy-autotrophy transition. *Frontiers in Plant Science* **5**: 400.

Zienkiewicz A, Zienkiewicz K, Poliner E, Pulman JA, Du ZY, Stefano G, Tsai CH, Horn P, Feussner I, Farre EM *et al.* 2020. The microalga Nannochloropsis during transition from quiescence to autotrophy in response to nitrogen availability. *Plant Physiology* **182**: 819–839.

Supporting Information

Additional Supporting Information may be found online in the Supporting Information section at the end of the article.

Dataset S1 Annotation file for gene.

Dataset S2 Annotation file for transposable elements.

Fig. S1 Global contribution of *Fragilariopsis* barcodes (V9) to diatom populations across the *Tara* Oceans expedition.

Fig. S2 Results from the physiological, biochemical, cytometry and protein analysis in *Fragilariopsis cylindrus*.

Fig. S3 SEM images and TEM image analysis of *Fragilariopsis cylindrus* in light and dark conditions.

Fig. S4 3D reconstruction of cells of *Fragilariopsis cylindrus* using focused ion beam-scanning electron microscopy (FIB-SEM).

Fig. S5 Fluorescence micrograms of *Fragilariopsis cylindrus* stained with DAPI and NileRed.

Fig. S6 Tracking genes significantly differentially expressed at single time points in *Fragilariopsis cylindrus*.

Fig. S7 Western blot targeting the active form of RNA Polymerase II (RPB1 CTD Ser2p) in *Fragilariopsis cylindrus*.

Fig. S8 Principal component analysis of a total of 17 light and dark transcriptomes of *Fragilariopsis cylindrus* from cultures in the acclimation phase in full light (T0LIGHT), in prolonged darkness (1 month), and upon return to light (up to 7 d).

Table S1 Summary and timing of the parameters measured from the cultures of *Fragilariopsis cylindrus*.

Table S2 Global contribution of Fragilariopsis barcodes (V9) to diatom populations across Tara Oceans.

Table S3 ID of genes of *Fragilariopsis cylindrus* included within each DREM subclusters and associated enriched GO categories.

Table S4 Complete list of genes of *Fragilariopsis cylindrus* that are significantly differentially expressed at single time points as compared to T0LIGHT.

Table S5 Correspondence of gene names in *Fragilariopsis cylindrus* with acronyms, the number of genes considered and the subcellular predictions from Fig. 5.

Table S6 Complete list of genes explored in *Fragilariopsis cylindrus*.

Video S1 FIB-SEM-Light-1: 3D reconstruction of a full-light-acclimated cell allowed with focused ion beam/scanning electron microscopy.

Video S2 FIB-SEM-Light-2: 3D reconstruction of a full-light-acclimated cell allowed with focused ion beam/scanning electron microscopy.

Video S3 FIB-SEM-Light-3: 3D reconstruction of a full-light-acclimated cell allowed with focused ion beam/scanning electron microscopy.

Video S4 FIB-SEM-Dark-1: 3D reconstruction of a dark-acclimated cell allowed with focused ion beam/scanning electron microscopy.

Video S5 FIB-SEM-Dark-2: 3D reconstruction of a dark-acclimated cell allowed with focused ion beam/scanning electron microscopy.

Video S6 FIB-SEM-Dark-3: 3D reconstruction of a dark-acclimated cell allowed with focused ion beam/scanning electron microscopy.

Please note: Wiley is not responsible for the content or functionality of any Supporting Information supplied by the authors. Any queries (other than missing material) should be directed to the *New Phytologist* Central Office.